AGU PUBLICATIONS

Geophysical Research Letters

RESEARCH LETTER
10.1002/2015GL066050

Key Points:
- Argo float data show that the EAC and its eddies have freshened over 2005–2012
- There is no warming of the EAC and eddies in neither Argo, nor XBT, nor model fields
- The freshening is caused by increased precipitation off Eastern Australia

Supporting Information:
- Figure S1
- Figure S2
- Figure S3
- Figure S4
- Figure S5
- Figure S6
- Figure S7
- Figure S8
- Figure S9
- Figure S10

Correspondence to:
T. Rykova,
tatiana.rykova@csiro.au

Citation:
Rykova, T., and P. R. Oke (2015), Recent freshening of the East Australian Current and its eddies, *Geophys. Res. Lett.*, *42*, 9369–9378, doi:10.1002/2015GL066050.

Received 3 SEP 2015
Accepted 20 OCT 2015
Accepted article online 28 OCT 2015
Published online 11 NOV 2015

Recent freshening of the East Australian Current and its eddies

Tatiana Rykova[1] and Peter R. Oke[1]

[1]CSIRO Oceans and Atmosphere Flagship, Hobart, Australia

Abstract The East Australian Current (EAC) has a relatively weak mean flow and an energetic eddy field that dominates the circulation. The properties of the mean flow have been studied in detail, but the changes in the eddy field have received little attention. We analyze Argo temperature and salinity profiles for 2005–2012 to construct a picture of the time-mean and time-varying properties of EAC eddies. We find that eddies and the surrounding waters of the western Tasman Sea are freshening at a rate of 0.017–0.025 practical salinity unit/yr over the top 100 m, with no significant temperature change. Consistent with the observations, fields from an eddy-resolving ocean model show freshening, with no temperature trend. Moreover, the model results indicate that observed changes are significant in the context of the variability over the last 20 years and may be part of a multiyear (perhaps decadal) cycle. We attribute the freshening of the region to increased precipitation off Eastern Australia.

1. Introduction

Western boundary currents (WBCs) are important for the transport of heat, salt, and other properties from low to high latitudes [e.g., *Ganachaud and Wunsch*, 2000]. WBCs are reported to be warming faster than the interior of ocean gyres [e.g., *Wu et al.*, 2012]. The East Australian Current (EAC), one of the major WBCs, receives less attention than other WBCs—particularly those in the Northern Hemisphere [e.g., *Imawaki et al.*, 2013]. The EAC, however, is reported to be warming at a rate that is higher than anywhere else in the Southern Hemisphere [e.g., *Holbrook and Bindoff*, 1997; *Ridgway and Dunn*, 2007], consistent with the acceleration and/or southward shift of the South Pacific Gyre [e.g., *Oke and England*, 2004; *Cai et al.*, 2005; *Cai*, 2006; *Ridgway*, 2007].

The EAC is characterized by a relatively weak mean flow [*Godfrey et al.*, 1980] and a very energetic eddy field [e.g., *Ridgway and Godfrey*, 1994; *Ridgway and Dunn*, 2003; *Bowen et al.*, 2005; *Mata et al.*, 2006]. South of the separation point the flow is mainly composed of eddies carrying EAC water that mixes with Tasman Sea water [e.g., *Olson*, 1991; *Everett et al.*, 2012]. The mean state and the spatial variability of the EAC itself to the north of the separation point have been studied in detail [e.g., *Ridgway and Godfrey*, 1994; *Marchesiello and Middleton*, 2000; *Ridgway*, 2007]. Previous studies have focused on various aspects of temporal EAC variability [e.g., *Cresswell and Legeckis*, 1986; *Mata et al.*, 2000; *Suthers et al.*, 2011, and references therein], including variability of the EAC on climate timescales [e.g., *Hill et al.*, 2011]. However, only relatively few studies have focused on EAC eddies. These include an eddy census, quantifying the biophysical properties of eddies in the so-called "Eddy Avenue" [*Everett et al.*, 2012], a model-based study that identified eddy characteristics in the Tasman Sea [*Brassington et al.*, 2011], observations of submesoscale anticyclonic lenses sampled by gliders [*Baird and Ridgway*, 2012], a case study in a large-amplitude cyclonic eddy [*Oke and Griffin*, 2011], and a study of changes in the poleward heat transport by eddies [*Cetina-Heredia et al.*, 2014]. A series of modeling studies estimate possible changes in the EAC eddy field using a downscaled climate projection for possible 2060s conditions [*Sun et al.*, 2012; *Matear et al.*, 2013; *Oliver and Holbrook*, 2014]. Specifically, *Matear et al.* [2013] suggest that there may be an increase in eddy activity in the Tasman Sea, with a 1° southward shift of the EAC separation point, and *Oliver and Holbrook* [2014] suggest that there may be a 3°C Tasman Sea-wide warming and an increase in the EAC eddy transport in the future. EAC warming not only has important consequences for the ocean circulation and water properties distribution but also affects biological species that populate the South Australian waters [e.g., *Poloczanska et al.*, 2007; *Johnson et al.*, 2011; *Matear et al.*, 2013].

To date, no studies have focused on the freshwater budget of the EAC or its eddies. However, on a global scale, *Durack et al.* [2012] examined the hydrological cycle using *in situ* data, showing that there has been an amplification of both surface and subsurface variability: showing that salinity has increased in

the evaporation-dominated regions in all the ocean basins and enhanced freshening has occurred in the precipitation-dominated regions. More locally, *Cravatte et al.* [2009] observed freshening of the tropical Pacific over the last 50 years. These findings are relevant to, and consistent with, the results presented in this paper.

In this study we aim to describe the characteristics of a mean EAC cyclonic and anticyclonic eddy from Argo data, considering the water column down to 2000 m. We aim to document their seasonal and interannual variability, detecting the changes in the eddies, explaining them, and putting them in the context of the EAC variability. Moreover, we seek to determine whether the *in situ* measurements that have reported warming off the east coast of Tasmania, at Maria Island (~43°S) [*Ridgway*, 2007], relate to a warming of the whole EAC region, the entire Tasman Sea, or whether it could be explained by a southward shift of the EAC extension [e.g., *Oke and England*, 2004; *Cai et al.*, 2005].

In this study we combine all available Argo float data in the EAC region between 2005 and 2012 with satellite altimetry to assess the changes in the cyclonic and anticyclonic eddies in the western Tasman Sea. We detect pronounced surface and subsurface (down to 200 m) freshening (with no significant change in temperature) of both cyclonic and anticyclonic eddies over the Argo period. We augment an 8 year long Argo record with data from a repeat high-resolution expendable bathythermograph (XBT) section and data from an 18 year integration (from 1993 to 2012) of an eddy-resolving ocean general circulation model (that realistically reproduces the low-frequency ocean circulation) [*Oke et al.*, 2013] to assess the interannual changes in the state of the EAC itself. We further explain the observed freshening in the EAC and its eddies by looking at local and remote forcing. Using gridded estimates of precipitation (http://precip.gsfc.nasa.gov) and fluxes from an atmospheric reanalysis (ERA-Interim), we show that precipitation off eastern Australia increased between 2005 and 2012 at a rate that explains up to 90% of the observed freshening. We find consistency between the Argo, XBT, and model fields that all show no significant warming on the timescales that we consider.

The paper is structured as follows: Argo, altimetry, XBT, and surface flux data are described in section 2. The method of assigning data from Argo floats to eddies and some technical details of obtaining the typical cyclonic and anticyclonic eddy and their time series are described in section 2.1. Section 3 describes the mean eddy properties, using Argo data, and their variability over an 8 year period. A summary and discussion is presented in section 4.

2. Data and Methods

2.1. Observations

To understand the mean properties and interannual variability of eddies in the EAC region, we use observed temperature and salinity profiles from the Argo array, in combination with satellite-based gridded sea level anomaly (SLA) from Archiving Validating Interpretation of Satellite Oceanographic (AVISO) data [*Ducet et al.*, 2000]. The AVISO gridded SLA maps are generated by objectively mapping along-track SLA from all available altimeter missions onto a 1/3° near-global grid.

We objectively "link" each Argo profile to the nearest cyclonic and anticyclonic eddy using the method described in detail in supporting information. Briefly, using gridded SLA fields, we identify the closest local maximum and minimum in SLA that is located within 250 km of each Argo float. We regard these SLA extrema as the central location of the closest eddies, and we consider only eddies with SLA extrema exceeding 0.2 m. We also restrict our analysis to the region of high variability, where the standard deviation of SLA exceeds 0.2 m. We then determine whether each float is within an eddy. A profile is considered to be within a cyclonic (anticyclonic) eddy if the SLA immediately above the float is less (greater) than −0.02 m (+0.02 m), and if the SLA decreases (increases) monotonically between the location of the float and the location of the nearest SLA minimum (maximum) at the time of the observation. Finally, we visually inspect the SLA field around each float, to check that this objective linkage between floats and eddies is appropriate. We provide several examples in the supporting information, demonstrating how the method works for a number of different scenarios (see Figures S1–S4 in the supporting information). Note that we chose not to exploit any of the widely used databases of eddy statistics (e.g., http://cioss.coas.oregonstate.edu/eddies/) [*Chelton et al.*, 2011] because they did not meet our specific needs (with assumptions about, for example, eddy size and duration). Using our simple, albeit labor-intensive, approach, we identify 765 temperature and salinity profiles in cyclonic eddies and 1749 profiles in anticyclonic eddies for the period from 2005 to 2012. We restrict our analysis to this period because prior to 2005 we regard the density of Argo floats to be too sparse in the

Tasman Sea to be reliable for our purposes. The Argo data used here have been quality controlled by the Argo team, and manually quality controlled with all unrealistic profiles (e.g., convectively unstable) excluded.

As part of this study, we are trying to understand whether the observed changes in Tasman Sea eddies are related to changes in the properties of the EAC itself. To assess the long-term trend in the EAC temperature, we use data from PX30 [*Roemmich et al.*, 2005]—a high-density XBT section between Brisbane, Australia, and New Caledonia. We use 88 quality-controlled XBT sections, between 1991 and 2013 (approximately quarterly sampling) through the core of the EAC at ~26°S between the coast and 158°E, with horizontal sampling of 10–20 km.

2.2. Ocean Model

The key result from this study is based exclusively on observations. However, to understand the context of the observed changes, we complement our analysis with the fields from an eddy-resolving ocean model. The model is version 3 of the Bluelink Ocean Forecasting Australia Model (OFAM3) [*Oke et al.*, 2013], a near-global configuration of the Modular Ocean Model [*Griffies et al.*, 2004). The model has a 5 m vertical resolution near the surface that gradually increases to 10 m resolution by 200 m depth and is coarser below that. The horizontal grid spacings are 1/10° for all longitudes and for latitudes from 76°S to 76°N. Below 2000 m depth the model is restored to annual climatological mean values of temperature and salinity using fields from the CSIRO Atlas for Regional Seas (CARS) [*Ridgway and Dunn*, 2003], with a restoring timescale of 365 days, to avoid any drift in the deep ocean fields. For further details on the model configuration the reader is referred to *Oke et al.* [2013]. Note that in this study we only use the model fields to provide context for the analyzed observations, and to provide insights into the possible causes of the observed changes.

2.3. Atmospheric Fluxes

To understand the observed variability, we use gridded estimates of precipitation [*Adler et al.*, 2003] and estimates of surface fluxes from and an atmospheric reanalysis (ERA-Interim) [*Dee and Uppala*, 2009]. The gridded precipitation estimates are a monthly, near-global, 2.5° resolution product that combines observations from multiple satellites with rain gauge data. These fields are produced under the Global Precipitation Climatology Project (GPCP; precip.gsfc.nasa.gov; Version 2.2; accessed from www.esrl.noaa.gov/psd/data/gridded/data.gpcp.html). We also use monthly mean fields of heat and freshwater fluxes from ERA-Interim (accessed from http://data-portal.ecmwf.int/data/d/interim_daily/). This includes the shortwave radiation, net longwave radiation, sensible and latent heat fluxes, and the precipitation minus evaporation (PmE) fields. We compute the area average of precipitation, total heat flux (by first summing all four components), and precipitation minus evaporation for several regions described below.

2.4. Limitations

There are limitations to the observations used in this study. The spatial resolution of the Argo profiles does not resolve the mesoscale properly—with a profile nominally every 200–300 km. This means that we cannot resolve individual eddies properly. Instead, we combine profiles from different eddies to quantify properties and characteristics of a mean eddy. Similarly, the gridded SLA only represents the large eddies, owing to the 1/3° grid and the relatively long length-scales (about 200 km *e*-folding) used in the gridding. Comparisons with independent rain gauge observations indicate that the GPCP fields generally underestimate the in situ precipitation [*Adler et al.*, 2003]. The atmospheric reanalysis fields used here are from a state-of-the-art product, based on a data-assimilating model [*Dee and Uppala*, 2009], with the largest uncertainty in the precipitation and evaporation fields that are important for this study.

The method used here also has limitations. The thresholds for linking the temperature and salinity profiles to eddies are somewhat subjective (i.e., the required SLA above the float, and the cutoff of magnitude of the eddy's SLA extrema). However, we have repeated our analysis using different thresholds (see Figures S5 and S6 in the supporting information, showing results for eddies with SLA amplitudes of 0.2–0.4 m and >0.4 m), and we find the conclusions of the study to be insensitive to these parameters.

3. Results

3.1. Mean Eddy Sections

After linking Argo profiles to the eddies with maximum SLA magnitudes exceeding 0.2 m, we construct two estimates of the radial section through an average anticyclonic and cyclonic EAC eddy. The first method sorts the profiles by distance from the eddy center and averages profiles in 25 km bins. The second method sorts

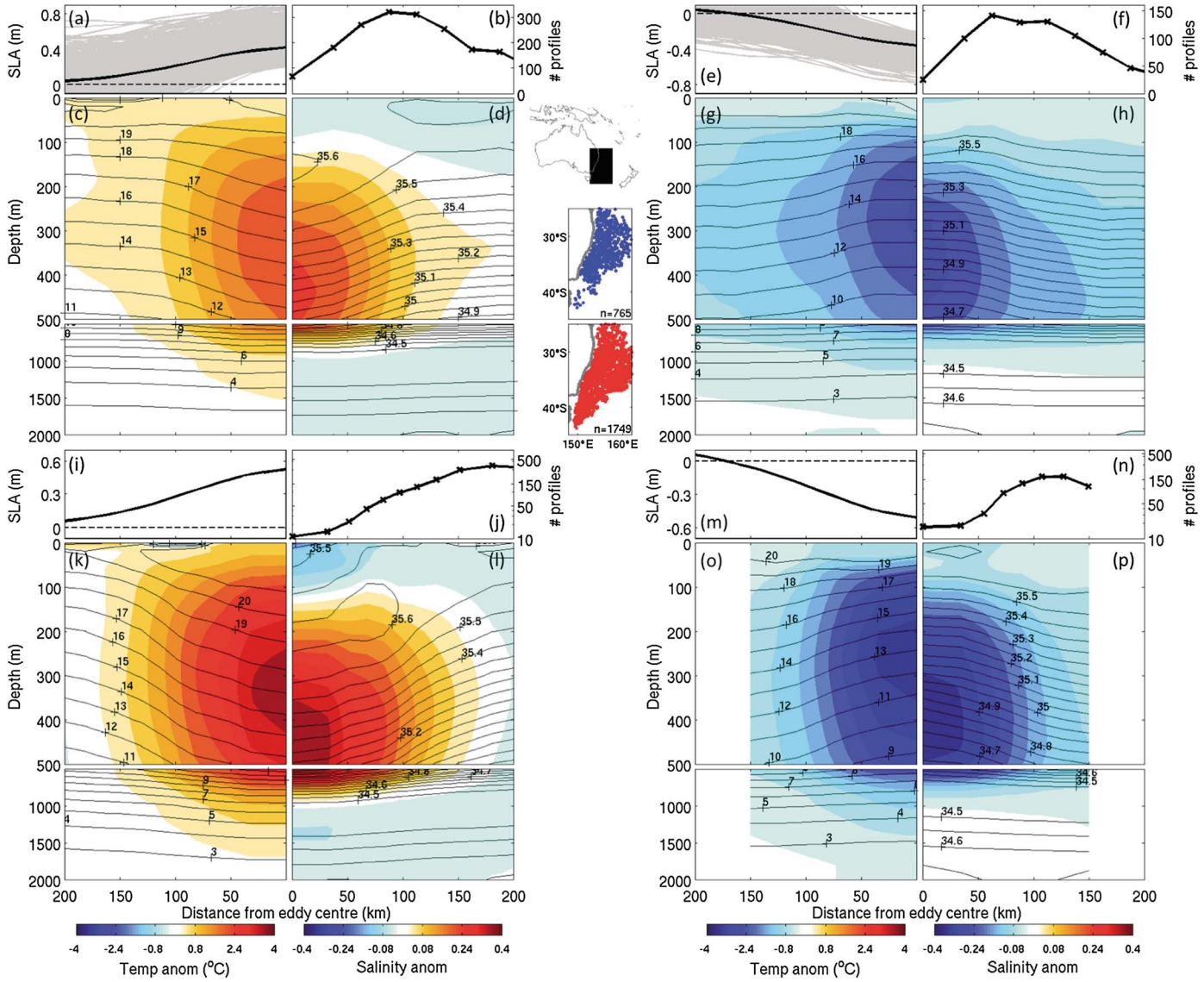

Figure 1. Sections of (a, e, i, and m) mean SLA and (b, f, j, and n) number of profiles, (c, g, k, and o) cross sections of mean temperature (contours) and temperature anomalies (color), and (d, h, l, and p) mean salinity (contours) and salinity anomalies (color) for anticyclonic (Figures 1a–1d and 1i–1l) and cyclonic (Figures 1e–1h and 1m–1p) eddies. The inset shows the region of interest and the number and location of profiles used to construct the mean cyclonic (blue) and anticyclonic (red) eddies. Figures 1a–1h show estimates constructed using profiles sorted as a function of distance from the eddy center, and Figures 1i–1p show estimates constructed using profiles sorted as a function of SLA above each profile.

the profiles by SLA immediately above each float and averages profiles in 0.06 m bins. The averaged profiles from the second method are then remapped into physical space, using a scaled SLA section, taken from the average section between floats and eddy centers. The first method is the simplest approach, but it tends to blend fields from strong and weak eddies somewhat inappropriately. The second method is more analogous to normalizing the eddies to the mean SLA section. The fields associated with these estimates, including the SLA section, the distribution of profiles, and the radial sections of potential temperature and salinity (contours), including their anomalies (color), are shown in Figure 1. Results from the first method are presented in Figures 1a–1h, and results from the second method are presented in Figures 1i–1p. The anomalies displayed in Figure 1 are computed by subtracting a seasonal climatology (using CARS) [*Ridgway and Dunn*, 2003] from each profile, using the location of each float and time of year when each profile was measured. The results are qualitatively similar for the two methods, but the fields from method two show stronger anomalies.

The mean anticyclonic eddy (Figures 1c, 1d, 1k, and 1l) has a warm and saline core, with maximum anomalies of 2–4°C centered around 300–350 m depth and 0.2–0.4 practical salinity unit (psu) centered at about

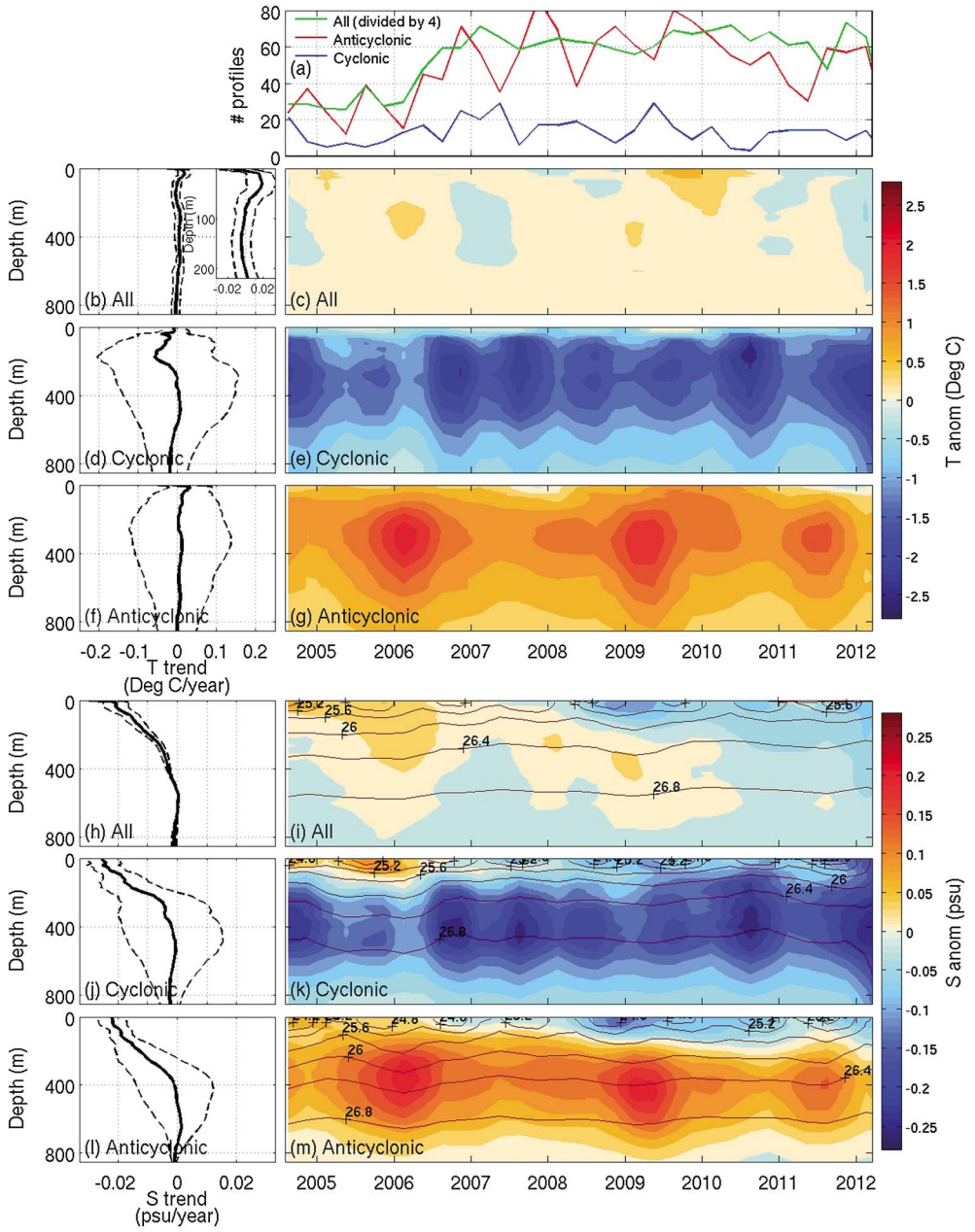

Figure 2. (a) Number of profiles per quarter in cyclonic (blue), anticyclonic (red) eddies, and using all profiles (green) in the high-variability region of the Tasman Sea and profiles of the (b, d, f, h, j, and l) linear trend and (c, e, g, i, k, and m) time series for temperature (Figures 2b–2g) and salinity (Figures 2h–2m) anomalies for different cases, as labeled in each panel. The profiles of linear trend include the 95% confidence limits.

400–450 m depth. The mean eddy is warmest at the surface and most saline at 150–200 m depth. The salinity and temperature anomalies are significant over the top 1000 m. Isotherms and isohalines are vertically displaced from the background by about 100–200 m. The heat content of the mean EAC anticyclone defined by the contour of 0.1 kg m^{-3} potential density anomaly is 2.3–4.1 × 10^{20} J. Following the methodology used by others [e.g., *Morrow et al.*, 2004], we multiply the heat content of the mean eddy by the reported number of EAC anticyclones per year (1–4 per year) [*Nilsson and Cresswell*, 1980; *Bowen et al.*, 2005; *Mata et al.*, 2006; *Wilkin and Zhang*, 2007; *Zavala-Garay et al.*, 2012], yielding an estimate of the poleward heat transport associated with anticyclonic eddies to be 0.01–0.06 PW. This is roughly 8–46% of the 0.13 PW of heat transport estimated to be entering the Tasman Sea [*Ridgway and Godfrey*, 1994].

The mean cyclonic eddy (Figures 1g, 1h, 1o, and 1p) has a cold and fresh core, with maximum anomalies of over −1.5 to −4°C centered around 250–350 m depth and −0.2 to −0.4 psu centered at about 300 m and 400 m depth. The mean eddy is warmest at the surface, with a colder core at depth, and has a subsurface salinity maximum at about 50 m. The salinity and temperature anomalies are significant over the top 1000 m and 2000 m, respectively. Isotherms and isohalines are vertically displaced from the background by about 50–125 m.

For both anticyclonic and cyclonic eddies, there is a change in sign of the salinity anomaly at about 1000 m depth. This is due to the heave (vertical uplift/depression) of isotherms and isohalines associated with Antarctic Intermediate Water, characterized by temperatures of 3–7°C and a salinity minimum of less than 34.5 psu.

3.2. Seasonal and Interannual Variability

EAC eddies, both cyclones and anticyclones, have a seasonal cycle that mainly consists of two seasons: "summer" (spanning Austral summer and fall) and "winter" (spanning Austral winter and spring). We find that *T* and *S* surface differences between Austral summer and Austral fall are less than 0.5°C and 0.03 psu for both anticyclonic and cyclonic eddies. Similarly, the differences between Austral winter and Austral spring are equally small. By contrast, the surface *T* and *S* differences between winter and summer are about 2(3)°C and 0.1(0.05) psu for anticyclonic (cyclonic) eddies. Both types of eddies are warmer and fresher in summer and colder and saltier in winter.

To quantify the interannual variability, we collate eddy profiles into quarterly bins and apply a weak temporal smoothing, using a three-point boxcar filter. Time series of the temporal variability of temperature and salinity fields, as a function of time and depth, are shown in Figures 2e, 2g, 2k, and 2m. On average, there are about 10 (40) profiles per quarter for cyclonic (anticyclonic) eddies (Figure 2a). The time series of anomalies using all available Argo profiles in the high-variability region of interest (Figures 2c and 2i) are also shown.

The time series in Figure 2 show anomalies from a seasonal climatology (using CARS; again using the location and time of year for each profile to convert *T*/*S* observations into anomalies). We note that the anomalies for the cyclonic eddies still show a seasonal cycle, with a maximum cold and fresh anomaly in Austral summer. No seasonal cycle is clearly evident in the time series for anticyclonic eddies or in the time series using all profiles. The EAC is the strongest toward the end of Austral summer [*Ridgway and Godfrey*, 1997; *Schiller et al.*, 2008], when the eddies are spawned from the stronger, more unstable EAC flow (although we acknowledge that there are different views on EAC seasonality and eddy formation [e.g., *Wilkin and Zhang*, 2007]). Cyclonic eddies typically only last for a few months [e.g., *Chelton et al.*, 2011], so by Austral winter many of the cyclonic eddies have decayed. As a result, the anomaly profiles in the cyclonic eddies show a seasonal cycle. By contrast, anticyclonic eddies often last for more than a year [e.g., *Nilsson and Cresswell*, 1980], subject to merging with other anticyclonic eddies, so they are prolific throughout the year. As a result, the profiles in the anticyclonic eddies do not show a clear seasonal cycle.

The most noteworthy feature in Figure 2 is the freshening (most evident near the surface) that is especially pronounced after 2007 for both types of the EAC eddies. We quantify this freshening by computing the linear trends as a function of depth for each time series (Figures 2b, 2d, 2f, 2h, 2j, and 2l). This indicates that there is no significant warming evident in the Argo profiles for this region but that freshening is significant in the time series of eddy properties and in the time series of Tasman Sea properties using all profiles. The freshening is statistically significant over the upper 400 m using all Argo profiles, and over the upper 200 m in the eddies. To further quantify and understand the freshening, we show the time series of the temperature and salinity anomalies, averaged over the top 100 m in Figures 3b and 3c. The freshening since 2007 is clear in both cyclonic and anticyclonic eddies and in the time series using all Argo floats, with trends of -0.025 ± 0.006 psu/yr, -0.017 ± 0.003 psu/yr, and -0.018 ± 0.003 psu/yr, respectively (where the error bars denote the 95% confidence interval). By contrast, there is no significant trend in temperature in any of the time series considered.

To understand the cause of the freshening and to shed some light on the absence of warming, we examine time series of gridded precipitation [*Adler et al.*, 2003], and the total heat flux and precipitation minus evaporation (PmE) in various regions over the Pacific and Southern Oceans (see Figure 3a showing low-pass-filtered PmE anomaly). The heat flux (not shown) has only a weak negative trend after 2005 off eastern Australia (-0.35 ± 0.21 W/m^2/yr). However, the PmE anomaly field has a significant positive trend, indicating stronger

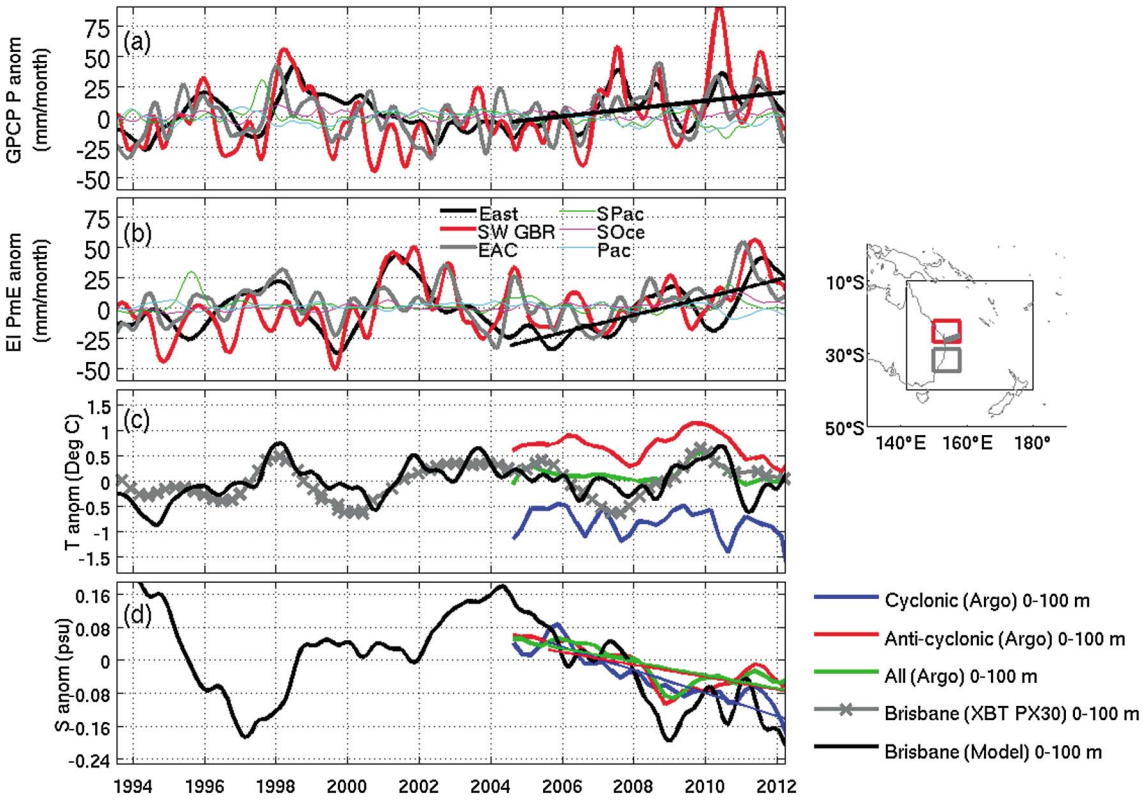

Figure 3. Time series of (a) spatially averaged precipitation anomaly (GPCP) and (b) precipitation minus evaporation anomaly (ERA-Interim) off eastern Australia (black box on the map), over the SGBR (red box), EAC region (grey box), the South Pacific (between the equator and 45°S), the Southern Ocean (south of 45°S), and the Pacific Ocean (north of 45°S); (b) temperature anomaly and (c) salinity anomaly for the model EAC off Brisbane (black; 153–156°E, 27–29°S), from XBT observations (temperature only; west of 158°E; denoted by the grey line with crosses—section denoted on map), cyclonic eddies (blue), anticyclonic eddies (red), and from all profiles (green), averaged over the top 100 m. Straight lines in Figures 3–3c) show the least squares fit to the data for the period 2005–2012.

precipitation and/or less evaporation. The trend of the PmE off eastern Australia is 4 ± 1 mm/month/yr after 2002. The trend of the PmE off eastern Australia is 7 ± 0.8 mm/month/yr between 2005 and 2012. Consistent with the estimates from the atmospheric reanalysis (ERA-Interim), the GPCP precipitation estimates off eastern Australia also show a positive trend, showing a linear trend of 3.2±0.5 mm/month/yr between 2005 and 2012. Integrating the GPCP precipitation anomalies off eastern Australia (2.7–3.7 mm/month/yr) over 1 year implies the addition of 0.032–0.044 m of freshwater to the ocean. If that additional freshwater is mixed/diffused over the top 100 m of the ocean, the implied freshening trend is 0.011–0.016 psu/yr. These estimates are of the same order as the observed freshening in the Argo data (which was between 0.017 and 0.025 psu/yr), explaining up to 90% of the observed freshening. We therefore conclude that the likely cause of the eddy freshening is consistent with increased precipitation and decreased evaporation off eastern Australia.

To understand the significance of the observed freshening and the lack of change in the Tasman Sea temperature, we present time series of modeled temperature and salinity anomalies, averaged between the surface and 100 m depth in the EAC core (153–156°E, 27–29°S; Figures 3b and 3c). To demonstrate the validity of the model results, we also show times series of observed temperature anomalies for the upper 100 m along PX30, west of 158°E. We show good consistency between the low-pass-filtered modeled and observed temperature. Although we cannot assess salinity in the same way (since XBT is temperature-only), we present a favorable comparison of the observed (using Argo) and modeled (using OFAM3) mean profiles of temperature and salinity anomalies in eddies in the EAC region in the supporting information (see Figure S6). Consistent with the Argo and XBT results, the model shows no significant trend in temperature, but a distinct freshening, with a trend of −0.02 ± 0.003 psu/yr after 2005 (the same order as the Argo observations). The model was forced by the same fluxes used to produce the fields in Figure 3a. This suggests that no changes in the temperature and the pronounced freshening, observed in the Argo data and reproduced in the model, are robust and can be largely explained by the change in PmE and insignificant changes in the heat fluxes.

Inclusion of the model results in Figure 3 is also intended to provide the reference for the observed changes. We note that the 8 year freshening (2005–2013) is significant compared to the preceding variability—only matched by a 4 year freshening between 1994 and 1998 that also corresponds to an increase in PmE off eastern Australia.

4. Discussion and Conclusions

It is important to understand the changes in the amount of heat and fresh water that are transported by the WBCs and their eddies from low to high latitudes. This particularly applies to the EAC region that is reported to be warming much faster than any other place in the Southern Hemisphere [e.g., *Holbrook and Bindoff*, 1997; *Ridgway and Dunn*, 2007]. The strength of the EAC and the shift in its southward penetration accompanied by the changes in the wind field have been analyzed in previous studies [e.g., *Ridgway*, 2007]. Temperature and salinity changes in the EAC have mainly been documented based on satellite sea surface temperature [e.g., *Foster et al.*, 2014] and *in situ* observations from a 60 year record off Maria Island, far downstream of the EAC core [*Ridgway*, 2007]. No assessment of the hydrographic changes of eddies has been previously reported from observations; however, the changes in global freshwater cycle have been discussed by *Durack et al.* [2012] and are consistent with our findings. In this work we have looked at the interannual changes in the EAC and its eddies over the last 20 years using the data from Argo floats and satellite altimetry (2005–2012) complemented by model results (1993–2012) and XBT data to provide the context for the observed changes.

A central result of this study is a reconstruction of the mean EAC anticyclonic and cyclonic eddy from *in situ* data. The only existing knowledge up to date was based on the limited hydrographic or XBT sections and modeling studies [e.g., *Ridgway et al.*, 2008; *Oke and Griffin*, 2011]. Here we show the properties of the typical EAC eddies from Argo float data and investigate their variability.

We find that both cyclonic and anticyclonic eddies, as well as the EAC itself, are getting fresher, particularly over the 5 year period between 2007 and 2012, and especially over the top 100 m. These trends are seen both in the short Argo float record and in the longer record reconstructed from the model that agrees well with observations in the period of overlap. We attribute the freshening to surface fluxes, with PmE increasing markedly after roughly 2007. These changes in the eddies and the Tasman Sea are consistent with the recent findings by *Cravatte et al.* [2009] who observe freshening of the tropical Pacific as well in the previous 50 years.

The freshening of shallow waters in the western Tasman Sea could have significant biological implications. As *Baird et al.* [2011] discuss, the fresh water at the surface of the anticyclones corresponds to higher concentrations of chlorophyll *a* in the euphotic zone. Freshening of the Tasman Sea may therefore lead to higher productivity in the region.

The results presented above indicate that there is no significant warming of either the EAC itself or its eddies evident in the Argo observations since 2005. At first glance, this appears to contradict the recent reports by *Ridgway* [2007] and *Foster et al.* [2014]. However, we note that *Ridgway* [2007] used *in situ* data prior to 2002 and satellite data prior to 2005. Moreover, *Foster et al.* [2014] used satellite sea surface temperature observations to quantify temperature trends around Australia, reporting "marginal warming" of the EAC—when in fact they show (their Figure 3) no statistically significant warming in the EAC eddy region. We confirm this in our study, showing time series from XBT in the core of the EAC with no significant warming—with a trend of -0.006 ± 0.004°C/yr (i.e., weak cooling at PX30) between 1991 and 2013 and 0.039 ± 0.011°C/yr between 1995 and 2013. By contrast, *Foster et al.* [2014] show significant warming to the south of the EAC eddy region, consistent with the findings of *Ridgway* [2007] and also consistent with a southward shift of the South Pacific subtropical gyre as reported by *Cai et al.* [2005].

The observational record used to examine the hydrographic changes of EAC eddies is too short to draw conclusions on the longer-term trends of the region. But the magnitude of the observed interannual variability is greater than expected, and it is in itself important. It is possible that the observed freshening is part of a multiyear cycle (perhaps decadal). A longer observational record is needed to further explore this. Indeed, the observed freshening reported in this paper has significant implications for the stability of EAC eddies—acting to stabilize them via increased stratification—and also possibly for biological productivity of the Tasman Sea.

Acknowledgments
The authors gratefully acknowledge input from K. Ridgway and two anonymous reviewers that led to improvements in this work. Profile data used in this study were collected and made freely available by the International Argo Program and the national programs that contribute to it (www.argo.ucsd.edu,argo.jcommops.org). The Argo Program is part of the Global Ocean Observing System. XBT data are made freely available on the Atlantic Oceanographic and Meteorological Laboratory, funded by the NOAA Office of Climate Observations, and by the Scripps High Resolution XBT program (www-hrx.ucsd.edu). The GPCP (precip.gsfc.nasa.gov) combined precipitation data (version 2.2; accessed from www.esrl.noaa.gov/psd/data/gridded/data.gpcp.html in October 2015) were developed and computed by the NASA/Goddard Space Flight Center's Laboratory for Atmospheres as a contribution to the GEWEX Global Precipitation Climatology Project.

References

Adler, R. F., et al. (2003), The version-2 Global Precipitation Climatology Project (GPCP) monthly precipitation analysis (1979–present), *J. Hydrometeorol.*, *4*(6), 1147–1167.

Baird, M. E., and K. R. Ridgway (2012), The southward transport of sub-mesoscale lenses of Bass Strait Water in the centre of anti-cyclonic mesoscale eddies, *Geophys. Res. Lett.*, *39*, L02603, doi:10.1029/2011GL050643.

Baird, M. E., I. Suthers, D. A. Griffin, B. Hollings, C. B. Pattiaratchi, J. D. Everett, M. Roughan, K. Oubelkheir, and M. A. Doblin (2011), The effect of surface flooding on the physical-biogeochemical dynamics of a warm-core eddy off southeast Australia, *Deep Sea Res.*, *58*(5), 592–605.

Bowen, M. M., J. L. Wilkin, and B. Emery (2005), Variability and forcing of the East Australian Current, *J. Geophys. Res.*, *110*, C03019, doi:10.1029/2004JC002533.

Brassington, G. B., N. Summons, and R. Lumpkin (2011), Observed and simulated Lagrangian and eddy characteristics of the East Australian Current and the Tasman Sea, *Deep Sea Res.*, *58*, 559–573.

Cai, W. (2006), Antarctic ozone depletion causes an intensification of the Southern Ocean super-gyre circulation, *Geophys. Res. Lett.*, *33*, L03712, doi:10.1029/2005GL024911.

Cai, W., G. Shi, T. Cowan, D. Bi, and J. Ribbe (2005), The response of the Southern Annular Mode, the East Australian Current, and the southern mid-latitude ocean circulation to global warming, *Geophys. Res. Lett.*, *32*, L23706, doi:10.1029/2005GL024701.

Cetina-Heredia, P., M. Roughan, E. Van Sebille, and M. Coleman (2014), Long-term trends in the East Australian Current separation latitude and eddy driven transport, *J. Geophys. Res. Oceans*, *119*, 4351–4366, doi:10.1002/2014JC010071.

Chelton, D. B., M. G. Schlax, and R. M. Samelson (2011), Global observations of nonlinear mesoscale eddies, *Prog. Oceanogr.*, *91*, 167–216, doi:10.1016/j.pocean.2011.01.002.

Cravatte, S., T. Delcroix, D. Zhang, M. McPhaden, and J. Leloup (2009), Observed freshening and warming of the western Pacific warm pool, *Clim. Dyn.*, *33*(4), 565–589.

Cresswell, G. R., and R. Legeckis (1986), Eddies off southeastern Australia, *Deep Sea Res.*, *33*(11-12), 1527–1562.

Dee, D. P., and S. Uppala (2009), Variational bias correction of satellite radiance data in the ERA-Interim reanalysis, *Q. J. R. Meteorol. Soc.*, *135*(644), 1830–1841, doi:10.1002/qj.493.

Ducet, N., P.-Y. L. Traon, and G. Reverdin (2000), Global high-resolution mapping of ocean circulation from TOPEX/POSEIDON and ERS-1 and-2, *J. Geophys. Res.*, *105*(C8), 19,477–19,498.

Durack, P. J., S. E. Wijffels, and R. J. Matear (2012), Ocean salinities reveal strong global water cycle intensification during 1950 to 2000, *Science*, *336*(6080), 455–458.

Everett, J. D., M. E. Baird, P. R. Oke, and I. M. Suthers (2012), An avenue of eddies: Quantifying the biophysical properties of mesoscale eddies in the Tasman Sea, *Geophys. Res. Lett.*, *39*, L16608, doi:10.1029/2012GL053091.

Foster, S. D., D. A. Griffin, and P. K. Dunstan (2014), Twenty years of high-resolution sea surface temperature imagery around Australia: Inter-annual and annual variability, *PloS one*, *9*(7), e100762.

Ganachaud, A., and C. Wunsch (2000), Improved estimates of global ocean circulation, heat transport and mixing from hydrographic data, *Nature*, *408*(6811), 453–457.

Godfrey, J. S., G. R. Cresswell, T. J. Golding, and A. F. Pearce (1980), The separation of the East Australian Current, *J. Phys. Oceanogr.*, *10*(3), 430–440.

Hill, K. L., S. R. Rintoul, K. R. Ridgway, and P. R. Oke (2011), Decadal changes in the South Pacific western boundary current system revealed in observations and ocean state estimates, *J. Geophys. Res.*, *116*, C01009, doi:10.1029/2009JC005926.

Holbrook, N. J., and N. L. Bindoff (1997), Interannual and decadal temperature variability in the southwest Pacific Ocean between 1955 and 1988, *J. Clim.*, *10*(5), 1035–1049.

Imawaki, S., A. S. Bower, L. Beal, and B. Qiu (2013), Western boundary currents. Ocean circulation and climate—A 21st century perspective, 305–338.

Johnson, C. R., et al. (2011), Climate change cascades: Shifts in oceanography, species' ranges and subtidal marine community dynamics in eastern Tasmania, *J. Exp. Mar. Biol. Ecol.*, *400*(1), 17–32.

Marchesiello, P., and J. H. Middleton (2000), Modeling the East Australian Current in the western Tasman Sea, *J. Phys. Oceanogr.*, *30*(11), 2956–2971.

Mata, M. M., M. Tomczak, S. E. Wijffels, and J. A. Church (2000), East Australian Current volume transports at 30 degrees s: Estimates from the world ocean circulation experiment hydrographic sections PR11/P6 and the PCM3 current meter array, *J. Geophys. Res.*, *105*(C12), 28,509–28,526.

Mata, M. M., S. E. Wijffels, J. A. Church, and M. Tomczak (2006), Eddy shedding and energy conversions in the East Australian Current, *J. Geophys. Res.*, *111*, C09034, doi:10.1029/2006JC003592.

Matear, R., M. Chamberlain, C. Sun, and M. Feng (2013), Climate change projection of the Tasman Sea from an eddy-resolving ocean model, *J. Geophys. Res. Oceans*, *118*, 2961–2976, doi:10.1002/jgrc.20202.

Morrow, R., F. Birol, D. A. Griffin, and J. Sudre (2004), Divergent pathways of cyclonic and anti-cyclonic ocean eddies, *Geophys. Res. Lett.*, *31*, L24311, doi:10.1029/2004GL020974.

Nilsson, C., and G. Cresswell (1980), The formation and evolution of East Australian Current warm-core eddies, *Prog. Oceanogr.*, *9*(3), 133–183.

Oke, P. R., and M. H. England (2004), Oceanic response to changes in the latitude of the Southern Hemisphere subpolar westerly winds, *J. Clim.*, *17*(5), 1040–1054.

Oke, P. R., and D. A. Griffin (2011), The cold-core eddy and strong upwelling off the coast of New South Wales in early 2007, *Deep Sea Res.*, *58*(5), 574–591, doi:10.1016/j.dsr2.2010.06.006.

Oke, P. R., et al. (2013), Evaluation of a near-global eddy-resolving ocean model, *Geosci. Model Dev.*, *6*, 591–615, doi:10.5194/gmd-6-591-2013.

Oliver, E., and N. Holbrook (2014), Extending our understanding of South Pacific gyre "spin-up": Modeling the East Australian Current in a future climate, *J. Geophys. Res. Oceans*, *119*, 2788–2805, doi:10.1002/2013JC009591.

Olson, D. B. (1991), Rings in the ocean, *Annu. Rev. Earth Planet. Sci.*, *19*, 283–311.

Poloczanska, E., et al. (2007), Climate change and Australian marine life, *Oceanogr. Mar. Biol.*, *45*, 407–478.

Ridgway, K. (2007), Long-term trend and decadal variability of the southward penetration of the East Australian Current, *Geophys. Res. Lett.*, *34*, L13613, doi:10.1029/2007GL030393.

Ridgway, K., and J. Godfrey (1994), Mass and heat budgets in the East Australian Current: A direct approach, *J. Geophys. Res.*, *99*(C2), 3231–3248.

Ridgway, K., R. Coleman, R. Bailey, and P. Sutton (2008), Decadal variability of East Australian Current transport inferred from repeated high-density XBT transects, a CTD survey and satellite altimetry, *J. Geophys. Res.*, *113*, C08039, doi:10.1029/2007JC004664.

Ridgway, K. R., and J. R. Dunn (2003), Mesoscale structure of the mean East Australian Current system and its relationship with topography, *Prog. Oceanogr.*, *56*(2), 189–222, doi:10.1016/S0079-6611(03)00004-1.

Ridgway, K. R., and J. R. Dunn (2007), Observational evidence for a Southern Hemisphere oceanic supergyre, *Geophys. Res. Lett.*, *34*, L13612, doi:10.1029/2007GL030392.

Ridgway, K. R., and J. S. Godfrey (1997), Seasonal cycle of the East Australian Current, *J. Geophys. Res.*, *102*(C10), 22,921–22,936.

Roemmich, D., J. Gilson, J. Willis, P. Sutton, and K. Ridgway (2005), Closing the time-varying mass and heat budgets for large ocean areas: The Tasman Box, *J. Clim.*, *18*(13), 2330–2343.

Schiller, A., P. R. Oke, G. B. Brassington, M. Entel, R. Fiedler, D. A. Griffin, and J. V. Mansbridge (2008), Eddy-resolving ocean circulation in the Asian-Australian region inferred from an ocean reanalysis effort, *Prog. Oceanogr.*, *76*(3), 334–365, doi:10.1016/j.pocean.2008.01.003.

Sun, C., M. Feng, R. Matear, M. Chamberlain, P. Craig, K. Ridgway, and A. Schiller (2012), Marine downscaling of a future climate scenario for Australian boundary currents, *J. Clim.*, *25*, 2947–2962, doi:10.1175/JCLI-D-11-00159.1.

Suthers, I. M., et al. (2011), The strengthening East Australian Current, its eddies and biological effects—An introduction and overview, *Deep Sea Res.*, *58*(5), 538–546, doi:10.1016/j.dsr2.2010.09.029.

Wilkin, J. L., and W. Zhang (2007), Modes of mesoscale sea surface height and temperature variability in the East Australian Current, *J. Geophys. Res.*, *112*, C01013, doi:10.1029/2006JC003590.

Wu, L., et al. (2012), Enhanced warming over the global subtropical western boundary currents, *Nat. Clim. Change*, *2*, 161–166, doi:10.1038/nclimate1353.

Zavala-Garay, J., J. Wilkin, and H. Arango (2012), Predictability of mesoscale variability in the East Australian Current given strong-constraint data assimilation, *J. Phys. Oceanogr.*, *42*(9), 1402–1420.